AMERICAN SOCIETY FOR MICROBIOLOGY | Journal of Virology®

VIRUS-CELL INTERACTIONS

Chemokine PF4 Inhibits EV71 and CA16 Infections at the Entry Stage

Zhichao Pei,[a] Hong Wang,[a] Zhilei Zhao,[a] Xiang Chen,[a] Chen Huan,[a] Wenyan Zhang[a]

[a]Center of Infectious Diseases and Pathogen Biology, Institute of Virology and AIDS Research, Key Laboratory of Organ Regeneration and Transplantation of The Ministry of Education, The First Hospital of Jilin University, Changchun, China

ABSTRACT Platelet factor 4 (PF4) or the CXC chemokine CXCL4 is the most abundant protein within the α-granules of platelets. Previous studies found that PF4 regulates infections of several viruses, including HIV-1, H1N1, hepatitis C virus (HCV), and dengue virus. Here, we show that PF4 is an inhibitor of enterovirus A71 (EV71) and coxsackievirus A16 (CA16) infections. The secreted form of PF4 from transfected cells or soluble purified PF4 from *Escherichia coli*, even lacking signal peptide affected secretion, obviously inhibited the propagation of EV71 and CA16. Mechanistically, we demonstrated that PF4 blocked the entry of the virus into the host cells by interactions with VP3 proteins of EV71/CA16 and the interaction with SCARB2 receptor-mediated EV71 and CA16 endocytosis. As expected, the incubation of anti-PF4 antibody with PF4 blocked PF4 inhibition on EV71 and CA16 infections further supported the above conclusion. Importantly, pretreatment of EV71 viruses with PF4 significantly protected the neonatal mice from EV71 lethal challenge and promoted the survival rate of infected mice. PF4 derived from natural platelets by EV71/CA16 activation also presented strong inhibition on EV71 and CA16. In summary, our study identified a new host factor against EV71 and CA16 infections, providing a novel strategy for EV71 and CA16 treatment.

IMPORTANCE The virus's life cycle starts with binding to cell surface receptors, resulting in receptor-mediated endocytosis. Targeting the entry of the virus into target cells is an effective strategy to develop a novel drug. EV71 and CA16 are the major pathogens that cause hand, foot, and mouth disease (HFMD) outbreaks worldwide since 2008. However, the treatment of EV71 and CA16 infections is mainly symptomatic because there is no approved drug. Therefore, the underlying pathogenesis of EV71/CA16 and the interaction between host-EV71/CA16 need to be further investigated to develop an inhibitor. Here, we identified PF4 as a potent entry inhibitor of EV71 and CA16 via binding to VP3 proteins of EV71 and CA16 or binding to receptor SCARB2. In the EV71 infection model, PF4 protected mice from EV71 lethal challenge and promoted the survival rate of EV71-infected mice. Our study suggests that PF4 represents a potential candidate host factor for anti-EV71 and CA16 infections.

KEYWORDS PF4, platelet activation, enterovirus, entry inhibition

Platelet factor 4 (PF4) or CXC chemokine (CXCL4) is a member of the CXC chemokine subfamily and secreted by platelets (1, 2). Platelets are anucleated blood cells and mainly maintain hemostasis (3, 4). Besides, platelets also mediate thrombosis and innate immune response and contribute to noncanonical functions of immune modulation, tissue repair, angiogenesis, regeneration, and metastasis (5–12). Platelets contain α and dense granules, contents of which are rich in cytokines such as C-X-C motif chemokine ligand (CXCL), C-C motif ligand (CCL), and transforming growth factor β (TGF-β) (13). Viral infection causes platelets activation that releases chemokines such as PF4, C-C chemokine ligand 5 (CCL5), and fibrinopeptides into the plasma, which play an important role in the replication and propagation of several viruses, including human immunodeficiency virus type I (HIV-1),

Editor Susana López, Instituto de Biotecnologia/UNAM

Address correspondence to Wenyan Zhang, zhangwenyan@jlu.edu.cn.

The authors declare no conflict of interest.

Received 14 March 2022
Accepted 25 April 2022
Published 17 May 2022

respiratory syncytial virus (RSV), H1N1 influenza, dengue virus (DV), and Japanese encephalitis virus (JEV) (14–20). PF4 has a dual role in HIV-1 infection, as it both inhibits and enhances HIV-1 replication (14, 19, 20). PF4 can induce monocyte differentiation into macrophages, while PF4-derived macrophages can be infected with macrophage-tropic HIV-1 (20). PF4 has been described as a broad-spectrum inhibitor to HIV-1 infections. The mechanism is that the PF4 blockade of HIV-1 infection occurs at the level of virus attachment and entry via directly binding to the HIV-1 envelope glycoprotein gp120 and its cell surface receptor C-X-C chemokine receptor type 4 (CXCR4) (14). PF4 is also involved in DV and JEV infections; that is, blocking PF4 significantly rescued production of alpha interferon (IFN-α), resulting in potent inhibition of the replication of both DV and JEV in monocytes (17, 18). PF4 was identified as a strong RSV restrictor by blocking virion attachment to heparin sulfate (HS) receptors, the main RSV receptor, while RSV infection induced elevated PF4 concentrations both in plasma and airway samples from mice and pediatric patients (16). It has also been reported that PF4 could resist enterovirus A71 (EV71) and herpes simplex virus 1 (HSV-1) infections, the two HS- dependent viruses (21, 22), but the underlying mechanism and PF4 broad-spectrum capacity against enterovirus family members are understudied.

Human enteroviruses (HEVs) belonging to the genus *Enterovirus* within the family *Picornaviridae* are divided into 13 species; 4 enterovirus species EV-A to D and 3 rhinovirus species A to C cause human diseases. EVs cause hand, foot, and mouth disease (HFMD), myocarditis, respiratory disease, and herpangina. EV-A includes at least 16 members with different serotypes of coxsackievirus (CV), such as coxsackievirus A6 (CA6), coxsackievirus A16 (CA16), and EV71 (23, 24). EV infection starts with binding to one or multiple cell surface receptors. Human scavenger receptor class B, member 2 (hSCARB2), as the major receptor, mediates entry of multiple EVs, including that of EV71, coxsackievirus A16, A7 and A14, and has been shown to bind to EV71 VP1 GH and VP2 EF loops (25–27). In addition, other molecules, such as P-selectin glycoprotein ligand-1 (PSGL-1), HS proteoglycans, sialylated glycan, annexin II, vimentin, the intercellular adhesion molecule 5 (ICAM5/telencephalin), fibronectin, and prohibitin, are used by different enteroviruses as receptors (22, 28–31).

In this study, we investigated the effect of PF4 on the replication of EV71 and CA16 and found that PF4 potently inhibits viral infections by blocking EV71 and CA16 attachment or entry into host cells. Mechanistically, as an inhibitor of EV71 and CA16, PF4 directly interacts with the VP3 proteins of EV71 and CA16 and also binds to the major receptor SCARB2 of EV71 and CA16. Our findings are helpful in understanding EV pathogenesis and developing a novel therapeutic strategy for EV71 and CA16 infections.

RESULTS

Overexpression of PF4 but not δsp-PF4 inhibits EV71 and CA16 replication in HEK293T cells. HEK293T cells were transfected with pPF4-HA or VR1012 vector as a negative control to investigate whether PF4 affects EV71 and CA16 infections and were then infected with EV71 and CA16 at multiplicity of infections (MOIs) of 0.05 and MOI 0.001, respectively. The VP1 protein levels of viruses in PF4 overexpression cells and culture supernatant were detected at 12, 24, 36, and 48 h by immunoblotting analysis (IB). The results showed that pPF4 overexpression suppressed VP1 protein levels of EV71 and CA16, especially at 36 h and 48 h postinfection (pi) (Fig. 1A and E). The VP1 mRNA levels of EV71 and CA16 quantified by reverse transcriptase quantitative PCR (RT-qPCR) analysis also showed similar results (Fig. 1B and F). PF4 is a secreted protein, while a PF4 mutant lacking the signal peptide (pδsp-PF4) leads to secretion failure. To determine whether the PF4 inhibitory effect is secretion dependent, we constructed a pδsp-PF4-HA expression vector and detected its inhibitory effect on EVs. HEK293T cells were transfected with pPF4-HA or pδsp-PF4-HA expression vector in different doses and then infected with EV71 and CA16 24 h posttransfection at MOIs of 0.05 and 0.001, respectively. We observed that overexpression of PF4 but not δsp-PF4 suppressed the replication of EV71 and CA16 by the detection of VP1 protein (Fig. 1C and G) and mRNA levels (Fig. 1D and H) by IB and RT-qPCR analysis, suggesting that PF4 secreted into the supernatant is required for EV71 and CA16 inhibition. These results indicate that PF4 inhibits EV71 and CA16 replication with secretion-dependent inhibition.

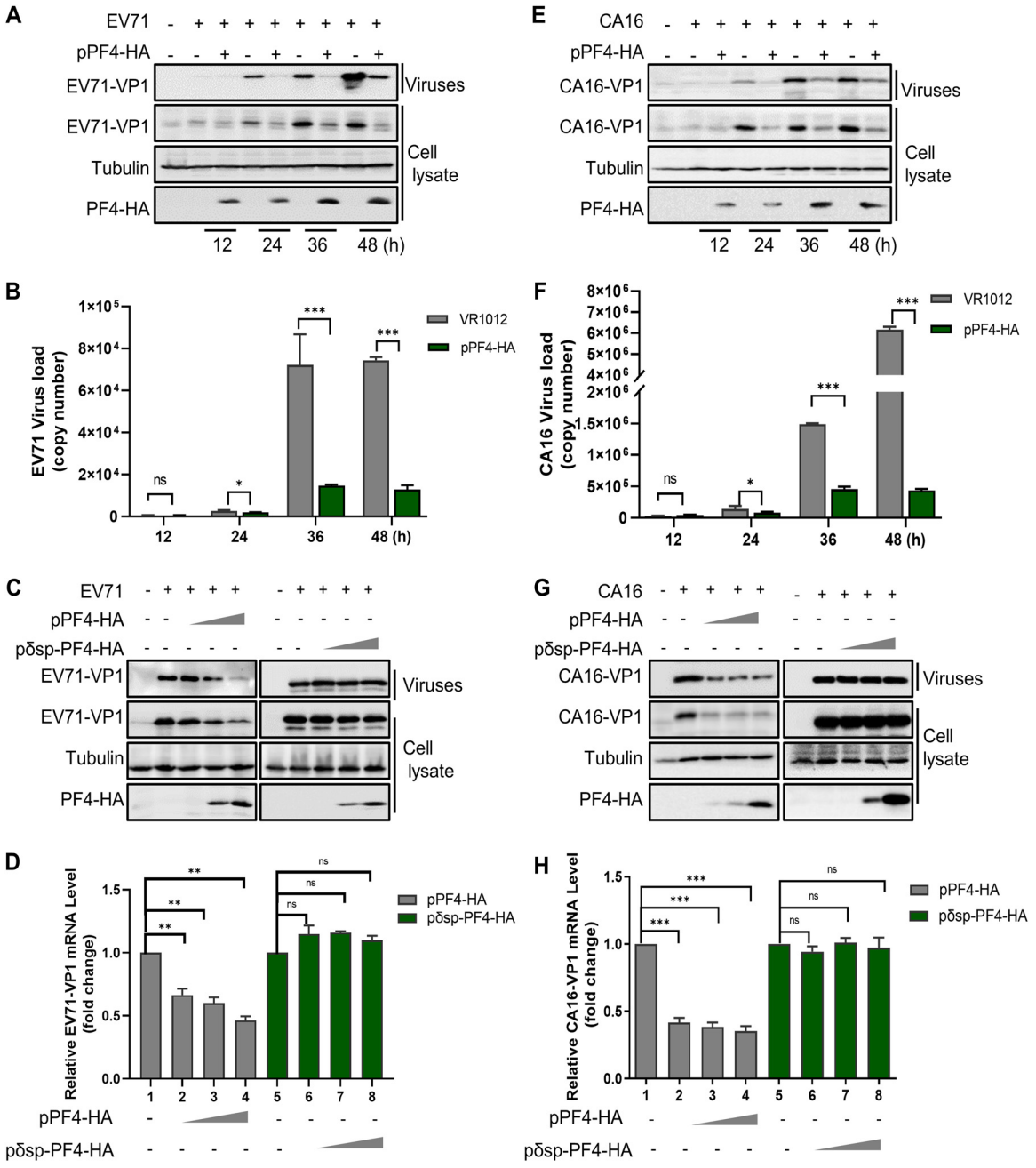

FIG 1 Overexpression of PF4 but not δsp-PF4 inhibits EV71 and CA16 infections. HEK293T cells were transfected with VR1012 and pPF4-HA (1,500 ng) expression vector for 24 h and then infected with EV71 (A and B) and CA16 (E and F) at MOIs of 0.05 and 0.001, respectively. At the indicated time points, the cells and culture supernatants were harvested. Immunoblotting (IB) analysis of EV71 (A) and CA16 (E) VP1 in cells was performed, with tubulin as a loading control. The VP1 protein in the supernatants was detected after ultracentrifugation. EV71 (B) and CA16 (F) viral RNA levels in cell lysates were detected by RT-qPCR with glyceraldehyde-3-phosphate dehydrogenase (GAPDH) as a control. The levels of viral RNA at 12 h, 24 h, 36 h, and 48 h were calculated by quantitative PCR (qPCR). The EV71-VP1 and CA16-VP1 plasmids were diluted for qPCR detection, and a standard curve was prepared to calculate the viral load of EV71/CA16 in the samples. HEK293T cells transfected with pPF4-HA or pδsp-PF4-HA expression vector were infected with EV71 (C and D) or CA16 (G and H) as indicated for 36 h. IB analysis of EV71 (C) and CA16 (G) VP1 in cells and culture supernatants; RT-qPCR analysis of EV71(D) and CA16 (H) viral mRNA levels in cell lysates. The viral mRNA levels of 100 ng, 300 ng, and 900 ng of pPF4-HA or pδsp-PF4-HA transfected cells was compared with cells transfected with VR1012. Results are representative of those from three independent repeats (mean ± standard deviation [SD]; *, $P < 0.05$; **, $P < 0.01$; ***, $P < 0.001$; ns, no significance; Student's *t* test).

Failure to secrete out from the cells leads to the failure of δsp-PF4 inhibition. HEK293T cells were transfected with VR1012, wild type (WT) pPF4-HA, or pδsp-PF4-HA, and the cell supernatant was collected and filtered with a 0.22-mm filter membrane. In the cell culture supernatant, the WT PF4 protein could be detected by both IB and

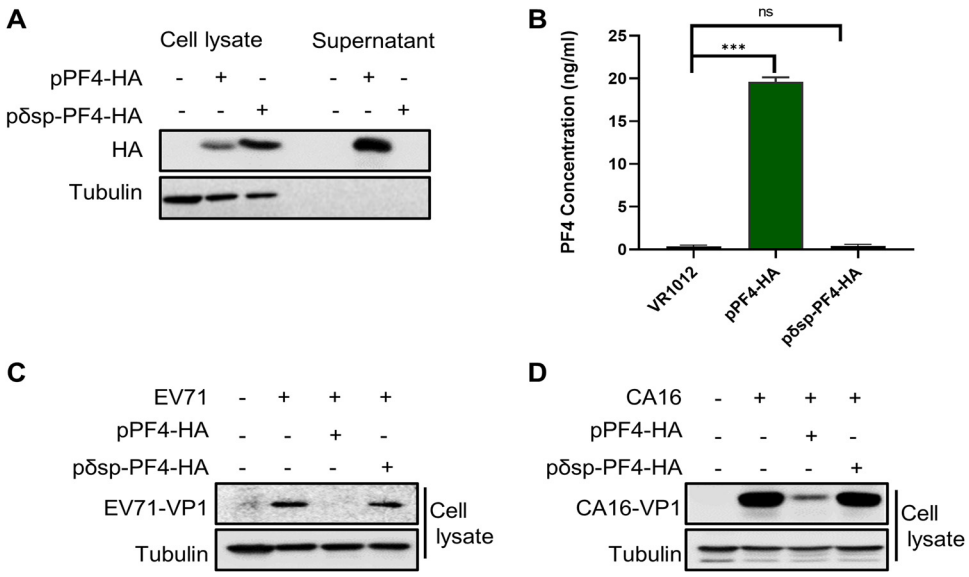

FIG 2 δsp-PF4 cannot inhibit EV71 and CA16 due to failure to secrete from the cells. HEK293T cells were transfected with VR1012, pPF4-HA, or pδsp-PF4 expression vector for 48 h, and then PF4 in cells and supernatant were detected by IB (A) and the concentration of PF4 was detected by ELISA (B). The culture supernatant obtained above was added to RD cells, incubated for 4 h, infected with EV71 and CA16 at MOIs of 0.01 and 0.05 respectively, and then washed twice before being cultured at 37°C with a new medium for 12 h. The EV71 (C) and CA16 (D) VP1 protein in RD cells was detected by IB. Results are representative of those from three independent repeats (mean ± SD; ***, $P < 0.001$; ns, no significance; Student's *t* test).

enzyme-linked immunosorbent assay (ELISA) methods, but the δsp-PF4 mutant failed to be detected (Fig. 2A and B), indicating that PF4 could secrete out from the transfected cells but δsp-PF4 could not. Rhabdomyosarcoma (RD) cells are sensitive to EV71 and CA16 infections, and we added the cell supernatant obtained above into the RD cells for 4 h; then, the cells were infected with EV71 and CA16 at MOIs of 0.01 and 0.05, respectively. Another 12 h later, the RD cells were collected to detect viral VP1 protein and mRNA levels. As expected, the supernatant from the WT PF4 transfected cells inhibited replication of EV71 and CA16, but that from δsp-PF4 transfected cells did not (Fig. 2C and D).

PF4 and soluble δsp-PF4 from *E. coli* inhibit the replication of EV71 and CA16 in a dose-dependent manner. To further determine whether the inhibition of PF4 on EV71 and CA16 replication is dose dependent, we collected the cell supernatants containing PF4 and added them to the RD cells in different concentrations for 4 h and then infected with EV71 or CA16, respectively. We observed that the increased dose of PF4 gradually reduced the VP1 protein level of EV71 (Fig. 3A) and CA16 (Fig. 3E) and the viral mRNA levels quantified by RT-qPCR analysis (Fig. 3B and F). As for δsp-PF4, His-tagged δsp-PF4 expressed in *Escherichia coli* were purified with a nickel column, quantified by ELISA, and then added into the RD cells in different concentrations. After 4 h of incubation, the RD cells were infected with EV71 and CA16 as described above. We also observed a similar inhibitory effect by detecting intracellular VP1 protein level and mRNA level in the supernatant (Fig. 3C, D, G to H), indicating that the soluble PF4 inhibits EV71 and CA16 in a dose-dependent manner.

Inhibition of PF4 on EV71 and CA16 occurs at the entry stage. To further investigate which stage of PF4 functions on EV71 and CA16 infections, we designed three assays as follows: (i) PF4 pretreatment in which PF4 was added to RD cells for 4 h before EV attachment, (ii) incubation treatment in which PF4 and EV were incubated for 4 h *in vitro* before being added to RD cells, and (iii) postentry treatment in which RD cells were infected with EV71 or CA16 for 4 h before PF4 was added (Fig. 4A). We observed that PF4 pretreatment and PF4 and EV incubation treatment both efficiently inhibited the replication of EV71 and CA16 by detecting the VP1 protein level and mRNA level in RD cells 12 hpi, whereas postentry treatment could not inhibit viral replication (Fig. 4B to E), suggesting that PF4 blocks viral entry via interaction with the receptor or interaction with the viral particle.

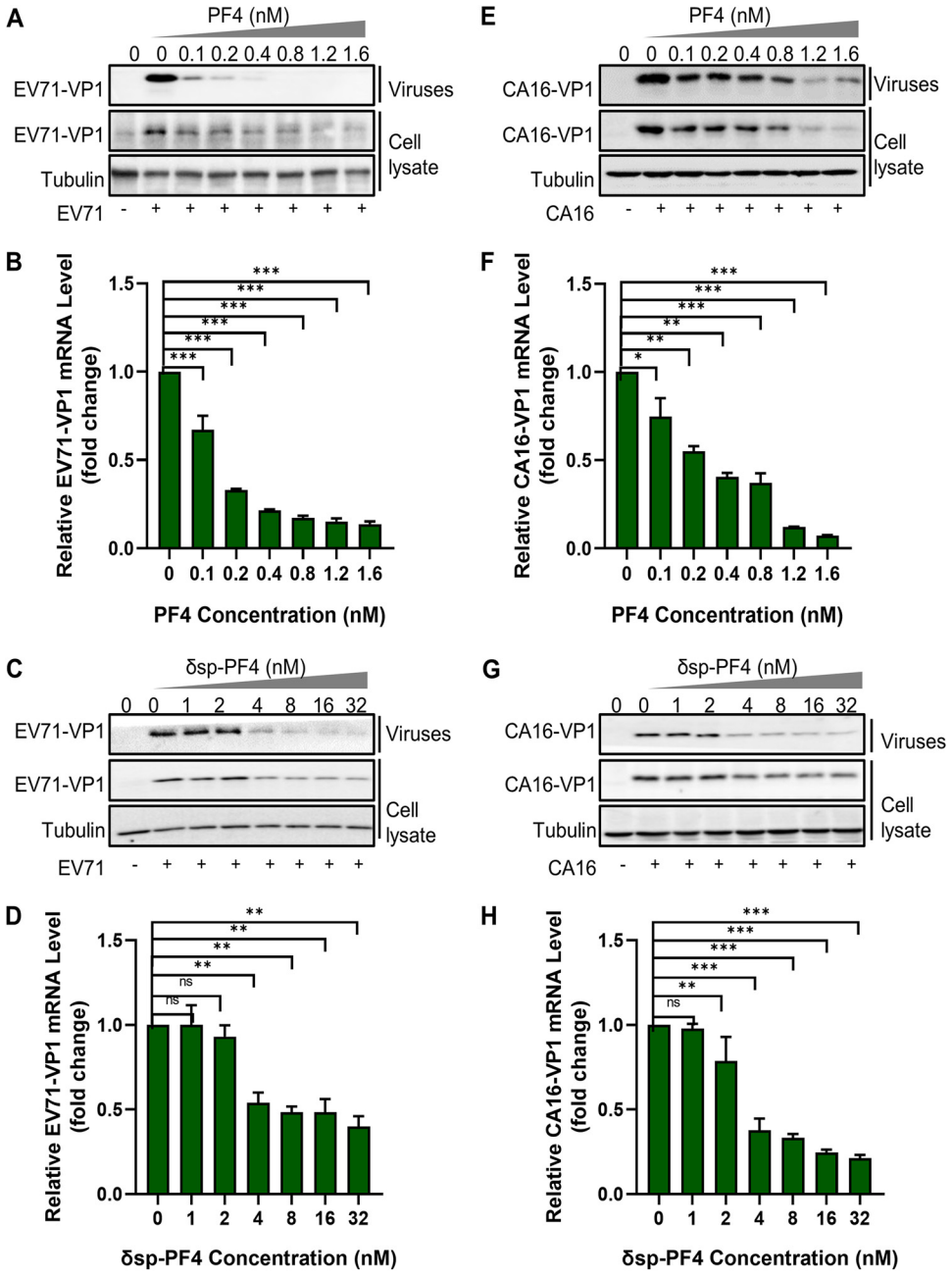

FIG 3 PF4 and soluble δsp-PF4 protein purified from *E. coli* inhibit EV71 and CA16. Incubation RD cells with the cell cultured supernatant in different concentrations of PF4 protein at a final concentration of 0, 0.1, 0.2, 0.4, 0.8, 1.2, and 1.6 nM for 4 h were infected with EV71 and CA16 at MOIs of 0.01 and 0.05 for 2 h and then washed twice with PBS. Twelve hours later, the cells and culture supernatants were harvested. IB analysis of EV71 (A) and CA16 (E) VP1 in cells and supernatants was performed. EV71 (B) and CA16 (F) viral RNA levels in cell lysates were detected by RT-qPCR with GAPDH as a control. Incubation RD cells with δsp-PF4 protein at a final concentration of 0, 1, 2, 4, 8, 16, and 32 nM for 4 h were then infected with EV71 and CA16 at MOIs of 0.01 and 0.05 for 12 h. IB analysis of EV71 (C) and CA16 (G) VP1 in cells and supernatants was performed. EV71 (D) and CA16 (H) viral mRNA levels in cell lysates were detected by RT-qPCR with GAPDH as a control. The level of viral mRNA of cells infected with virus alone was 1. Results are representative of those from three independent repeats (mean ± SD; **, $P < 0.01$; ***, $P < 0.001$; ns, no significance; Student's *t* test).

To confirm our speculation, we designed a binding assay of PF4 with the EV71/CA16 viruses and control by using PF4 antibody (Ab) to competitively bind to PF4. It has been reported that the SCARB2 is the cell membrane receptor of EV71 and CA16, so we used anti-SCARB2 Ab as a positive control. RD cells were pretreated with PF4, or PF4 and anti-PF4 Ab, or SCARB2 Ab for 2 h, followed by EV71 or CA16 binding. Bound viruses were measured

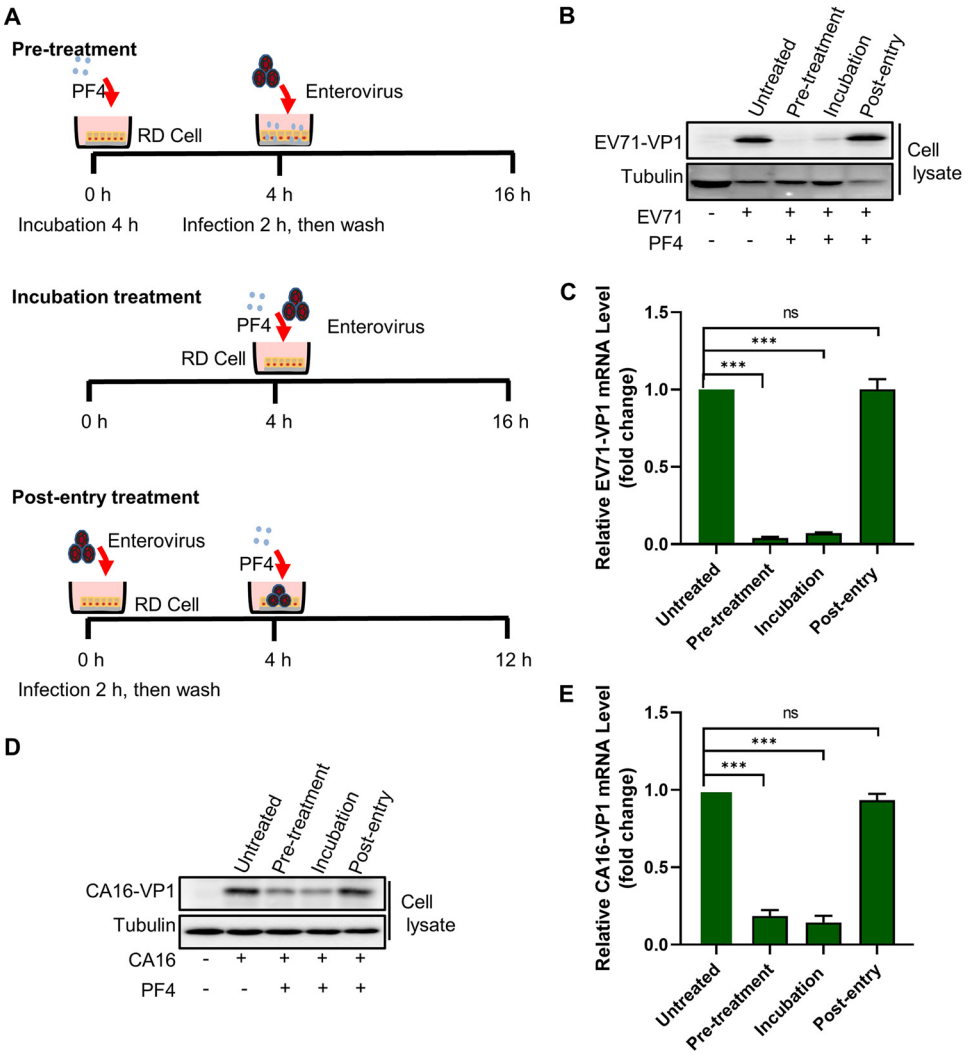

FIG 4 PF4 inhibits EV71 and CA16 at the entry step of infection. RD cells were infected with EV71 and CA16 at MOIs of 0.01 and 0.05, respectively, and treated with PF4 at −4, 0, and 4 hpi (A). With tubulin as a loading control, IB analysis of EV71 (B) and CA16 (D) VP1 protein in cells was performed. The levels of EV71 (C) and CA16 (E) viral mRNA in cell lysates were detected by RT-qPCR with GAPDH as a control. Results are representative of those from three independent repeats (mean ± SD; **, $P < 0.01$; ***, $P < 0.001$; ns, no significance; Student's *t* test).

by RT-qPCR. PF4 treatment blocked EV71 and CA16 attachment, whereas the inoculation of anti-PF4 Ab with PF4 rescued their attachment, indicating that EV71 and CA16 might bind to some surface factor of cells. As expected, anti-SCARB2 Ab also affects virus attachment (Fig. 5A and B). Moreover, pPF4 and pδsp-PF4 both did not affect the EV71 5' untranslated region (UTR) and CA16 5' UTR-driven luciferase activity, further supporting that pPF4 does not affect viral transcription (Fig. 5C and D). Altogether, these results suggest that PF4 acts in the entry stage of EV71 and CA16 infections, such as attachment or binding but not genome replication.

PF4 blocks EV71 and CA16 infections by binding to VP3. To determine the mechanism by how PF4 blocks EV71 and CA16 entry, we examined the interaction between PF4 and EV71/CA16 viral particles by coimmunoprecipitation assay (IP). The results showed that PF4 could pull down VP3 proteins of EV71 and CA16 very well, while few VP1 and VP2 proteins of EV71 and CA16 were pulled down by PF4 (Fig. 5E and F). We speculated that VP1/VP2 proteins of EV71 and CA16 can be indirectly pulled down a little by PF4 via binding to VP3. In order to confirm our speculation, we also detected the interaction of VP1, VP2, and VP3 of EV71 and PF4 by immunoprecipitating PF4 using cells cotransfected with PF4-HA, VP1-Flag, VP2-myc, and VP3-myc and observed a similar phenomenon (Fig. 5G). However, EV71 VP3 could pull

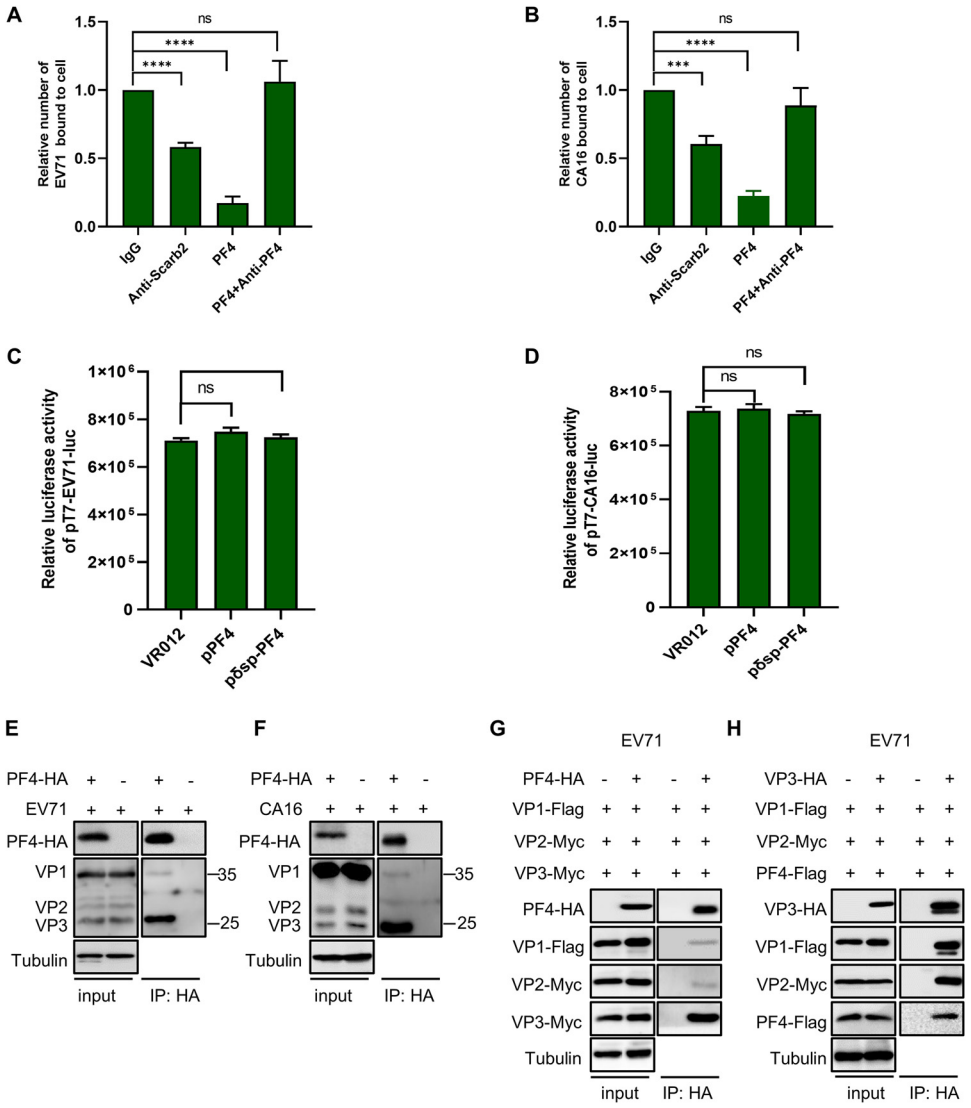

FIG 5 Binding assay. RD cells were pretreated with IgG (500 ng/mL), anti-SCARB2 antibody (300 ng/mL), PF4 (10 ng/mL), or PF4 (10 ng/mL) and anti-PF4 antibody (220 ng/mL) for 2 h and then washed with PBS, and the EV71 (A) or CA16 (B) was diluted in 2 mL DMEM and added to the cells at an MOI of 1 or 2, respectively, and then the cells were put on ice for 1 h, virus was removed and washed with PBS three times, and the cells were lysed in TRIzol for RNA analysis. PF4 did not affect the promoter activity of EV71 and CA16. Cotransfected HEK293T with pT7-EV71-Luc (C)/pT7-CA16-Luc (D), pT7 RNA polymerase, VR1012/pPF4/pδsp-PF4, and quantitation of reporter activity by a dual-luciferase reporter assay. (E and F) The interaction of PF4 with EV71 and CA16 viral particles. HEK293T cells were transfected with PF4-HA for 24 h and then infected with EV71 (E) or CA16 (F) at an MOI of 0.05, respectively. Another 24 h later, the cells were harvested and subjected to IP assay with hemagglutinin (HA) beads. IB was performed by using polyclonal anti-EV71 and anti-CA16 or anti-HA antibodies. (G) PF4 pulled down VP3 and a few VP1 and VP2 of EV71. HEK293T cells cotransfected with PF4-HA and EV71 VP1-Flag, VP2-Myc, and VP3-Myc as indicated were harvested at 48 h posttransfection and then subjected to IP assay with HA beads. Input and elution were detected by IB. (H) EV71 VP3 pulled down VP1, VP2, and PF4. HEK293T cells cotransfected with EV71 VP3-HA and VP1-Flag, VP2-Myc, PF4-Flag as indicated were harvested at 48 h posttransfection and subjected to IP assay with HA beads. Input and elution were detected by IB. Results are representative of those from three independent repeats (mean ± SD; ***, $P < 0.001$; ****, $P < 0.0001$; ns, no significance; Student's *t* test).

down VP1/VP2 and PF4 when VP3 was immunoprecipitated (Fig. 5H). Because VP1, VP2, and VP3 form the capsid surface by interacting with each other, we could not distinguish PF4 interaction with VP1, VP2, or VP3. Therefore, we next examined the interactions between PF4 with VP1, VP2, and VP3 proteins of EV71/CA16 separately by co-IP. The results showed that PF4 was coimmunoprecipitated by the VP3 proteins of EV71/CA16 and vice versa (Fig. 6A and B). δsp-PF4 protein also interacted with EV71/CA16 VP3 proteins (Fig. 6C). However, PF4-HA could not immunoprecipitate EV71/CA16 VP1-Flag and VP2-Myc proteins (Fig. 6D and E).

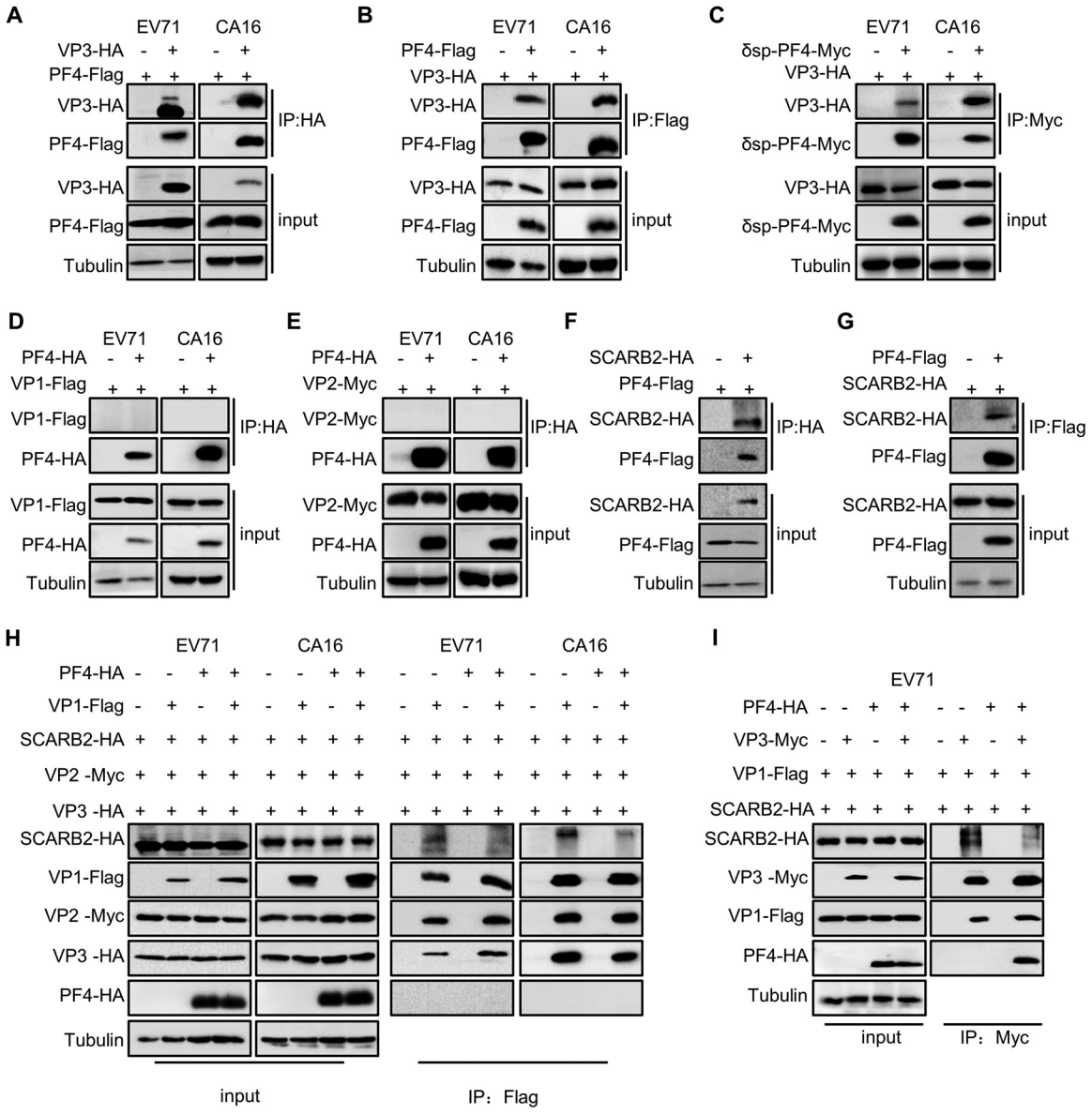

FIG 6 PF4 blocks EV71 and CA16 infection by binding to VP3 and SCARB2 proteins. (A and B) PF4 interacts with VP3 of EV71 and CA16. HEK293T cells cotransfected with PF4-HA and viral VP3-Flag were harvested at 48 h posttransfection and subjected to IP assay with HA beads (A) and Flag-protein G-agarose beads (B). Input and elution were detected by IB. (C) δsp-PF4 interacts with VP3 of multiple EVs. HEK293T cells were cotransfected with δsp-PF4-Myc and viral VP3-HA, harvested 48 h posttransfection, and subjected to IP assay with Myc-protein G-agarose beads. (D) PF4 did not interact with VP1 of EV71 and CA16. HEK293T cells cotransfected with PF4-HA and viral VP1-Flag were harvested at 48 h posttransfection and subjected to IP assay with HA beads. (E) PF4 did not interact with VP2 of EV71 and CA16. HEK293T cells cotransfected with PF4-HA and viral VP2-Myc were harvested at 48 h posttransfection and subjected to IP assay with HA beads. (F and G) PF4 interacts with SCARB2. Cells were cotransfected with PF4-Flag and SCARB2-HA as indicated and harvested 48 h posttransfection and then subjected to IP-HA assay with HA beads (F) or IP-Flag assay with Flag-protein G-agarose beads (G). (H and I) PF4 affects the binding of EV71 and CA16 capsid to SCARB2. HEK293T cells were cotransfected as indicated and harvested at 48 h posttransfection. IP was performed with Flag-protein G-agarose beads to immunoprecipitated VP1 (G) or with Myc-protein G-agarose beads to immunoprecipitated VP3 (I).

To examine whether the inhibitory effect of PF4 is associated with SCARB2, we examined the interaction of PF4 with SCARB2. The results showed that PF4 specifically interacted with SCARB2 and vice versa (Fig. 6F and G). To investigate whether PF4 presence affects the interaction of viral particles and SCARB2 receptor, we immunoprecipitated VP1 from cells cotransfected with VP1-Flag, VP2-Myc, VP3-HA, PF4-HA, and SCARB2-HA. The results showed that PF4 presence interfered with the interactions of EV71 and CA16 viral proteins with SCARB2, whereas PF4 was not pulled down by VP1 (Fig. 6H). To further illustrate this relationship, we immunoprecipitated EV71 VP3-myc from the cells cotransfected with

SCARB2-HA, EV71 VP1-Flag in the absence or the presence of PF4-HA (Fig. 6I). The results showed that EV71 VP3 could pull down VP1, PF4, and less SCARB2, further confirming that PF4 reduced the binding of VP3 with SCARB2. These results suggest that PF4 interacts with VP3 but not VP1 and VP2 proteins of EV71 and CA16 and also interacts with the SCARB2 receptor, thereby preventing EV71 and CA16 infections by blocking the binding of viral particles to SCARB2.

PF4 treatment in neonatal mice reduced EV71 infection and increased mouse survival. We previously established the neonatal mouse lethal infection model (32, 33). The antiviral activity of PF4 was evaluated in 1-day-old ICR mice. We first determined the toxicity of PF4 at a high dose of 2 ng/mL to the neonatal mice and a possible effective dose of 2 ng/mL on EV71 infection. PF4 alone (2 ng/mL, 10 μL/mouse), Changchun-circulating EV71 CC063 alone (each at $10^{5.5}$ 50% cell culture infective dose (CCID50 mL^{-1}), 10 μL/mouse), the inoculation of PF4 and CC063 (2 ng/mL PF4, 9 μL and 1 μL CC063 at $10^{5.5}$ $CCID_{50}$ mL^{-1}) for 1 h, or Dulbecco's modified Eagle medium (DMEM) negative control was separately intracerebrally injected into the neonatal mice. The neonatal mice were monitored and observed for 2 weeks. The results showed that the neonatal mice died from day 4, and all died by day 7 in only the EV71-infected group; the average clinical score was 5 on day 5. The PF4 treatment began to have forelimb paralysis on day 8 (Fig. 7A). Only a few mice died on day 12, and the survival rate on day 15 was 92% (Fig. 7B), suggesting that PF4 protected mice from EV71 lethal challenge. The PF4 alone had no toxicity even at high doses, suggesting that PF4 is safe *in vivo*. We next investigated whether PF4 inhibition on EV71 is dose dependent in neonatal mice. The incubation of PF4 (2 ng/mL, 1 ng/mL, or 0.7 ng/mL; 9 μL/mouse) with EV71 CC063 for 1 h *in vitro* or EV71 alone or DMEM negative control was intracerebrally injected into neonatal mice. PF4 presented dose-dependent protection from the EV71 challenge on clinical characteristics and mortality (Fig. 7C and D). PF4 treatment significantly improved clinical manifestations and survival rate, indicating that PF4 effectively protected neonatal mice against EV71 challenge *in vivo*.

To further prove the anti-EV71 effect of PF4, we detected viral mRNA levels in the brain, lungs, spinal muscles, and hind-limb muscle tissues of EV71-transfected mice. The results showed that viral mRNA levels of EV71 in the spine and hind-limb muscles in the PF4 treatment group were much lower than those in the EV71 infection group, and viral mRNA levels in the brain and lungs were slightly lower than those in the EV71 infection group (Fig. 7E). Meanwhile, lung, spine skeletal muscle, hind-limb muscle, and brain tissues of mice were sampled and histologically examined by hematoxylin and eosin (H&E) staining (Fig. 8). Compared to the negative control group, the lung tissue in the EV71-infected group was significantly solidified, the alveoli were fused to become pulmonary bullae, and muscle fibers were dissolved and broken. In the PF4 treatment group, especially the PF4 group at 2 ng/mL, the lung lesions and the rupture of the spine and hind-limb muscle tissues were much milder than those in the EV71 group. Altogether, these results demonstrate that PF4 can reduce the tissue lesions caused by EV71 and improve the survival rate of EV71-infected mice.

Platelet supernatant activated by EV71 and CA16 inhibits the replication of EV71 and CA16 *in vitro*. To confirm the effect of PF4 derived from natural platelets on virus replication, we collected platelets (1×10^7 cells) from the clinical blood sample and then activated with EV71 (10 μL at the concentration of 10^6 $CCID_{50}$ mL^{-1}) and CA16 (10 μL at the concentration of $10^{4.3}$ $CCID_{50}$ mL^{-1}) at 37°C for 4 h, respectively. The PF4 concentrations of platelet supernatant of EV71 and CA16 activated is 2.6 ng/mL and 2.5 ng/mL, respectively (Fig. 9A). We next treated RD cells with EV71/CA16 viruses alone, or EV71/CA16-activated platelet supernatant, or EV71/CA16-activated platelet supernatant plus anti-PF4 Ab for 2 h and then washed. Platelet supernatant alone was added into cells as a control. We observed that EV71/CA16-activated platelet supernatant could inhibit the replication of EV71 and CA16 by detecting the VP1 protein level in RD cells 24 hpi while adding anti-PF4 Ab could partially recover the antiviral effect of PF4 (Fig. 9B and C).

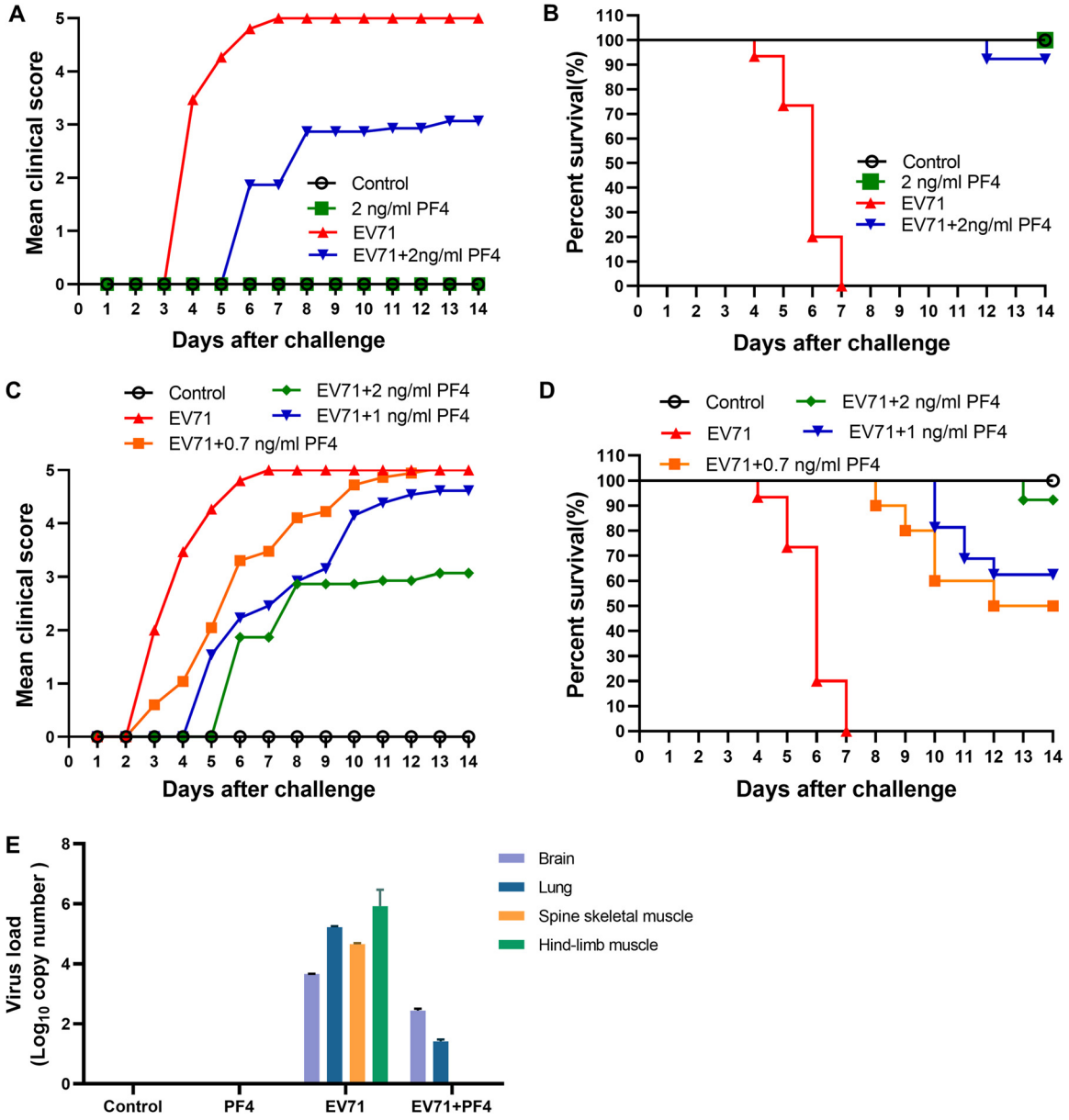

FIG 7 PF4 protects neonatal mice from EV71 lethal challenge. (A to D) The EV71 group, 1-day-old ICR mice (n = 13) were inoculated with 10 μL/mice of EV71 CC063 at $10^{5.5}$ $CCID_{50}$ mL^{-1}, DMEM (n = 13), and PF4 (n = 14). EV71 plus PF4 groups. PF4 (2 ng/mL, 1 ng/mL, or 0.7 ng/mL; 9 μL/mouse) was incubated with the EV71 CC063 (at $10^{6.5}$ $CCID_{50}$ mL^{-1}, 1 μL/mouse) for 1 h and then 1-day-old ICR mice were injected (n = 13, 16, or 10). Clinical scores and survival rates were monitored for 15 days postchallenge. Various grades of clinical disease were identified as follows: 0, healthy; 1, lethargy and inactivity; 2, wasting; 3, limb-tremor weakness; 4, hind-limb paralysis; and 5, moribund or dead. (E) Viral loads of EV71 in samples of the brain, lung, spine skeletal muscle, and hind-limb muscle tissues of infected mice were assessed by RT-qPCR on day 6. The results represent the mean virus load (log_{10} copies per milligram tissue) SDs (three mice per group, repeated three times).

DISCUSSION

PF4 is one of the abundant platelet chemokines and is secreted specifically by activated platelets. PF4 plays a complicated role in several viral infections. Studies have shown PF4 as a potent enhancer to HIV-1 infection in macrophage colony-stimulating factor (M-CSF)-derived macrophages and to both DV and JEV infection in monocytes (17, 19, 20). PF4 is also described as the broad-spectrum inhibitor to HIV-1, H1N1, and RSV infections (14–16). Despite the fact that the complicated function of PF4 in viral infection or immune response has been investigated, the role of PF4 during EV71 and CA16 infections is currently unknown. This study demonstrates that PF4 potently inhibits EV71 and CA16 infections in cells and a mouse infection model (Fig. 1 and 8). In transfected cells, PF4 inhibition is

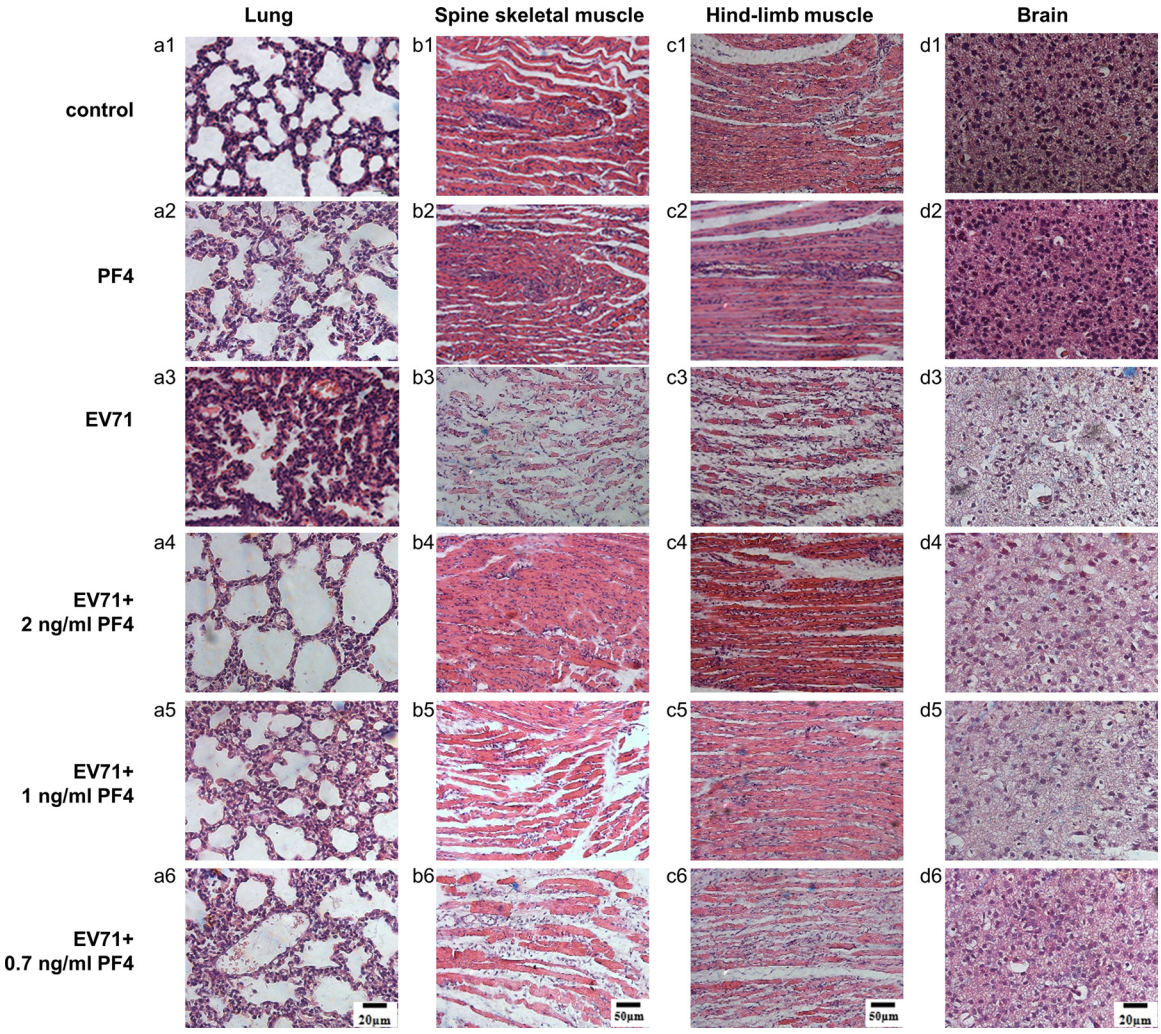

FIG 8 Pathology analysis of EV71-infected neonatal mice after PF4 treatment. One-day-old ICR mice were intracerebrally inoculated with DMEM (negative control), PF4 alone, EV71 CC063 ($10^{5.5}$ $CCID_{50}$ mL^{-1}) alone, or EV71 plus PF4 groups as described in Materials and Methods. Representative images from the lung (a1 to a6), spine skeletal muscle (b1 to b6), hind-limb muscle (c1 to c6), and brain (d1 to d6) postinfection are shown. The images for noninfected mice were used as a control (a1 and a2, b1 and b2, c1 and c2, and d1 and d2). Magnification, spine skeletal muscle, and hind-limb muscle, 200×; lung and brain, 400×.

secretion dependent; that is, the δsp-PF4 mutant lacking secretion signal failed to inhibit EV71 and CA16 infection (Fig. 2). Interestingly, soluble δsp-PF4 purified from *E. coli* was added to RD cells and showed a similar inhibitory effect to WT PF4. In addition, PF4 or δsp-PF4 could restrict EV71 and CA16 infection even at lower concentrations of 1.6 and 32 nM, respectively (Fig. 3). The above evidence hints that PF4 may act early by blocking viral entry. Auerbach et al. reported that HIV-1 inhibition of PF4 occurs at virus attachment and entry via direct interaction with the major viral envelope glycoprotein gp120 and HIV receptor CXCR4 (14). The other study indicated that only the secreted form of PF4 inhibits RSV replication (16). Therefore, we speculated that PF4 may bind to the viral particle or cell surface receptors to interfere with EV71 and CA16 attachment or entry.

We next designed three infection assays to confirm our hypothesis. Pretreatment RD cells with PF4 or inoculation of PF4 with EV71 and CA16 before being added into RD cells both inhibited EV71 and CA16 replication, whereas postentry assay showed PF4 failure to inhibit EV71 and CA16 infection, demonstrating that PF4 abrogates the entry of the virus into cells (Fig. 4). Moreover, anti-PF4 Ab abrogated PF4 inhibition, which further supports the above conclusion (Fig. 5). To investigate whether PF4 interacts with viral particles resulting in the blockage of virus entry, we examined the interaction between PF4 and the surface proteins VP1, VP2, and VP3 of EV71/CA16. Indeed, both PF4 and δsp-PF4 can interact with VP3 of

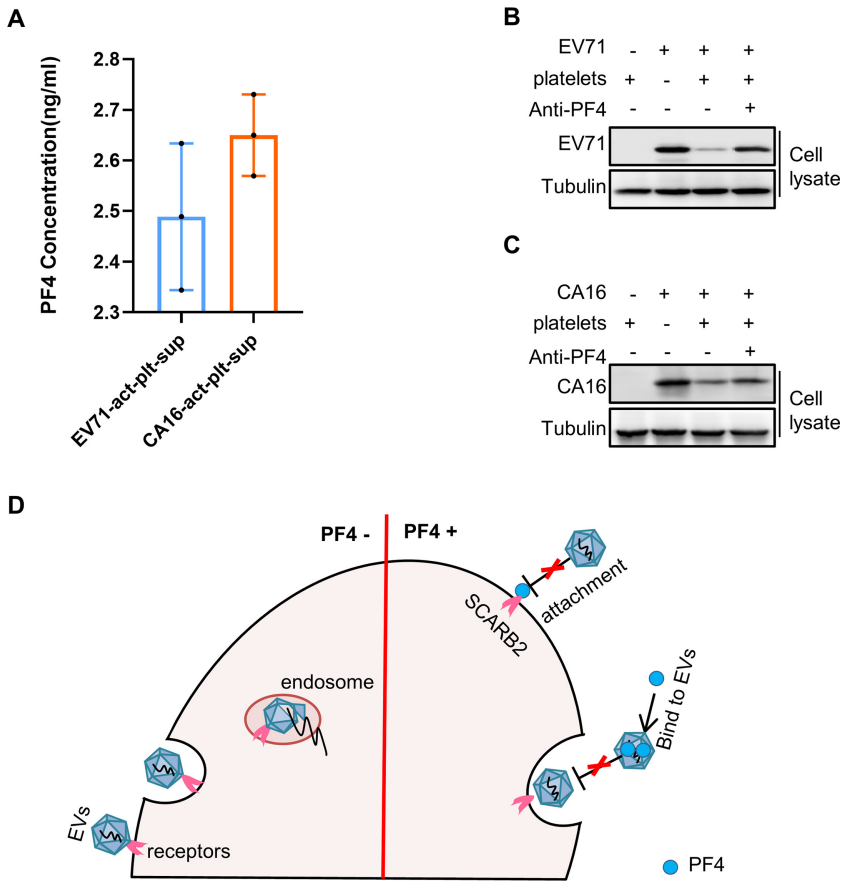

FIG 9 Natural platelet supernatant activated by EV71 and CA16 inhibits EV71 and CA16 infections. (A) Platelets were washed twice with Tyrode's solution and resuspended in 1 mL DMEM and then activated (1×10^7 cells) by EV71 (10^6 $CCID_{50}$ mL^{-1}, 10 μL) or CA16 ($10^{4.3}$ $CCID_{50}$ mL^{-1}, 10 μL) at 37°C for 2 h, respectively. The concentration of PF4 in the supernatant was measured by ELISA kit. (B and C) RD cells (2×10^5 cells/well, 12 wells) were added with EV71 or CA16 alone, or EV71/CA16-activated platelet supernatant, or EV71/CA16-activated platelet supernatant plus anti-PF4 (300 ng/mL) for 2 h and then washed. Platelet supernatant without virus activation was added into cells and used as a control. The cells were harvested after 24 h. (D) Proposed inhibition mechanism of chemokine PF4 on EV71 and CA16 attachment and entry. PF4 blocks EV71 and CA16 attachment and entry into target cells via interacting with the VP3 protein of EVs or interacting with receptor SCARB2.

EV71 and CA16 but not VP1 and VP2 of them (Fig. 6A to E). It is well known that EV71 and CA16 need to bind to the surface receptor of target cells and then enter into cells by receptor-mediated endocytosis (23). SCARB2 mediates not only attachment but also internalization and uncoating, whereas other receptors like PSGL-1 and HS proteoglycan only support viral attachment but cannot induce conformational changes in the virion that lead to uncoating (28). Moreover, a group of closely related viruses, EV71, CA16, CA14, and CA7, use SCARB2 as a major receptor (27). Thus, we detected the interaction between PF4 and SCARB2 receptors and demonstrated that PF4 could bind to SCARB2, which might be another reason why PF4 blocks virus attachment (Fig. 6F and G). Intriguingly, we observed that PF4 presence reduced the interaction of viral capsid with SCARB2 (Fig. 6H and I), whereas PF4 could not be pulled down by VP1 or even VP3 presence. Combined with the data shown in Fig. 5E to H, we concluded that PF4 interacts with the VP3 proteins of EV71/CA16 and receptor SCARB2 but not VP1 and VP2. Moreover, the interaction of PF4 with VP3 might occupy the domain of VP3 required for VP1 and VP2 interactions. Our data are similar to the mechanism that PF4 inhibits RSV replication by blocking RSV attachment to the receptor HS (16). It is worth noting that HS also mediates EV71 entry as a receptor, so it is possible that the interaction between PF4 and HS also blocks EV attachment to HS, which will be further investigated.

In addition, the genus *Enterovirus* contains diverse subtypes like CA6, CA10, and EVD68, which subsequently become a public health burden (34, 35). Whether PF4 possesses broad-spectrum antiviral properties is worth further investigation. In particular, the capsid of EVs and viral receptor are attractive targets for the development of small molecules that interfere with viral entry. Actually, we examined the effect of PF4 on other EVs and found a similar inhibitory effect (data not shown), but the underlying mechanism needs to be further discovered. After all, the VP3 sequence of different EVs are ~70% homology, so whether PF4 interacts with the VP3 of the diverse EVs also need to be confirmed. Accumulating evidence showed that the majority of peptides targeting the capsid of EVs or host targeting exhibited low anti-EV potency (micromolar range) (36), while PF4 showed stronger anti-EVs potency (nanomolar range), indicating the potential of PF4 as a candidate for the development of a new anti-EV therapeutic strategy.

Our previous studies have successfully established the EV71 lethal infection model (32). The preincubation of PF4 with EV71 viruses protected mice from EV71 lethal challenge and improved the survival rate of EV71-infected mice (Fig. 7). Compared to EV71-infected mice, PF4 treatment alleviated clinical symptoms, such as the inflammation of lung tissue, muscle bundle fracture, and dissolution of muscle fiber in spinal skeletal and hind-limb muscles (Fig. 8). Platelet-rich plasma obtained from healthy donors was centrifuged, and the platelets were resuspended and activated by EV71/CA16 infections to validate that PF4 plays a pivotal role in platelet activation for EV71 and CA16 inhibition. Platelet-activated supernatant could inhibit EV71 and CA16 replication, whereas PF4 Ab partially rescued EV71 and CA16 infections, indicating that PF4 is a major antiviral factor in platelet activation (Fig. 8B and C). Of course, other chemokines derived by platelet activation might also inhibit EV71 and CA16 replication, which is worth investigating in the future.

Based on our data, PF4 blocks EV71 and CA16 attachment or entry through two manners, and one is to bind to EV71 and CA16 VP3 proteins that block the interaction of virion particles with receptors. Another is to bind to the SCARB2 receptor that interferes with virion attachment, internalization, and uncoating (Fig. 8D). Therefore, PF4 plays a protective role in EV infections and is not the cause of immunopathology.

MATERIALS AND METHODS

Cell culture and viruses. HEK293T and RD cells were purchased from the American Type Culture Collection (ATCC) (Manassas, VA, USA; catalog numbers CRL-11268 and CCL-136). All cells were maintained in Dulbecco's modified Eagle medium (DMEM) (Gibco BRL, Grand Island, NY, USA), supplemented with 10% (vol/vol) fetal bovine serum (FBS) (Gibco), and cultured at 37°C with 5% CO_2. EV71 (CC063) and CA16 (shzh05-1) were described in a previous study (37).

Plasmid construction. The full-length PF4-HA/Flag was synthesized by the gene company, and the δsp-PF4-HA/Myc and δsp-PF4-His (truncation of PF4, 31 to 101 amino acids [aa]) were generated by amplification and inserting into VR1012 or pET-28a, respectively. The coding region of SCARB2 was generated by PCR amplification. The PCR product was digested with XbaI/BglII and cloned directly into the VR1012. pT7-EV71-Luc, pT7-CA16-Luc, and pT7 RNA polymerase vector were given by Jiang Chunlai (Jilin University). Viral VP1-Flag, VP2-Myc, and VP3-HA were amplified from viral RNAs and constructed into SalI/BamHI of VR1012. The primers used to construct these vectors are shown in Table 1.

Transfection and infection. HEK293T cells were seeded in a 12-well plate with 1×10^5/mL. According to the manufacturer's instructions, when cells were grown to approximately 70%, transfections were carried out by Lipofectamine 2000 (Invitrogen, Carlsbad, CA, USA). Using RD cells to amplify viruses, viruses were added into RD cells and grown for 48 h, and then all of the cells and supernatant were collected. The collected liquid was put in the −80°C refrigerator for 30 min, thawed at 37°C, with repeated freezing and thawing three times, filtered in a 0.22-mm filter, and stored in a −80°C refrigerator. For multiple EV viral infection, cells were grown to 70% confluence in a 12-well plate and incubated with the indicated strain at 37°C for 2 h at the indicated MOI and then washed twice with phosphate-buffered saline (PBS) and cultured at 37°C with new DMEM with 10% FBS.

RNA extraction and RT-qPCR. For RT-qPCR, RNA was extracted from HEK293T cells, RD cells, or tissues of mice samples with TRIzol reagent (Invitrogen) and then treated with DNase (Promega, Madison, WI, USA) before being quantitatively assayed. The cDNA was generated by a high-capacity cDNA reverse transcription kit (Applied Biosystems, Carlsbad, CA, USA). RT-qPCR was carried out on a Z480 instrument (Roche, Basel, Basel-City, SUI) with the real master mix (SYBR green kit; TaKaRa, Shiga, Japan) and primers described in the previous study (37). The RT-qPCR assay was carried out in a 20-μL volume consisting of 9 μL of 2× SYBR green solution, 1 μL of 5 μM/L of each oligonucleotide primer, and 2 μg of cDNA template. Amplification of the target fragment was carried out according to the following: 95°C for 1 min followed by 40 cycles of 95°C for 15 s and 55°C for 30 s.

Protein purification. δsp-PF4 protein with His tag was cloned into pET28a and expressed in an *E. coli* Transetta (DE3) chemically competent cell (TransGen Biotech, Beijing, China). The δsp-PF4 protein was

TABLE 1 Primers used in this study

Primer name	Sequence
PF4-Flag-F	TCGTCGACACCATGGACTACAAGGATGATGATGATAAGAGCTCCGCAGCCG
PF4-Flag-R	GTCCATGGTGTCGACGACGGTGACTGCAG
δsp-PF4-HA-F	AAGAAACTTTTGGAGAGTTACCCATACGACGTCCCAGACTACGCTTGAGGATCCAGATCTGCTG
δsp-PF4-HA-R	GTAACTCTCCAAAAGTTTCTTAATTATTTTCTTGTA
δsp-PF4-Myc-F	AAGAAACTTTTGGAGAGTGAGCAGAAACTCATCTCTGAAGAGGATCTGTAGGGATCCAGATCT
δsp-PF4-Myc-R	CTAACTCTCCAAAAGTTTCTTAATTATTTTCTTGTA
EV71-VP1-Flag-F	GCGTCGACATGGGAGATAGGGTGGCAGATG
EV71-VP1-Flag-R	CGGGATCCTCACTTGTCATCGTCGTCCTTGTAGTCAAGAGTAGTGATCGCTGTGC
EV71-VP2-Myc-F	GCGTCGACATGAAATCCCCGTCCGCTGAG
EV71-VP2-Myc-R	CGGGATCCTCACGCGTAATCTGGGACGTCGTAAGGGTATTGCGTGACTGCTTGCCTAAG
EV71-VP3-HA-F	GAAGATCTTCACGCGTAATCTGGGACGTCGTAAGGGTACCCTGGATGGTGCCCGTCTG
EV71-VP3-HA-R	GCGTCGACATGTTCCCCACCGAACTAAAAC
CA16-VP1-Flag-F	ACCATGGGGGATCCTATTGCAGATA
CA16-VP1-Flag-R	CAACGTTGTTATCTTGTCTCTACT
CA16-VP2-Myc-F	GCGCCAGGCAGTAAAGCAAGAGCAGAAACTCATC TCTGAAGAGGATCTGTGAGATCCAGATCTG
CA16-VP2-Myc-R	TCATTGCTTTACTGCCTGGCGCAGACCCGCAAATTCCGC
CA16-VP3-HA-F	ACCATGGGCATACCAACAGAGCTCAAAC
CA16-VP3-HA-R	TTGTATATTGGCCGTTTGCTCAA
SCARB2-HA-F	GCTCTAGAACCATGTACCCTTACGACGTCCCAGATTACGCG GGCCGATGCTG

purified with Ni-column affinity chromatography. The purity of the resulting δsp-PF4 protein was analyzed through SDS-PAGE analysis and ELISA kit (human PF4/CXCL4 ELISA kit; Frankel, Shanghai, China).

Virus entry assay. In the pretreatment group, RD cells were incubated with PF4 or δsp-PF4 protein in different concentrations at 37°C for 4 h and then infected with viruses for 2 h, washed with PBS twice, and incubated at 37°C for 12 h. In the incubation treatment, viruses and PF4 or δsp-PF4 protein were mixed and then added to the RD cells for 2 h, washed with PBS, and incubated at 37°C for 12 h. In the postentry treatment, RD cells were incubated with viruses for 2 h, washed with PBS, and incubated with PF4 or δsp-PF4 protein at 37°C for 10 h. PF4 was obtained from the supernatant of transfected HEK293T cells with pPF4-HA and then filtered with a 0.22-mm filter. δsp-PF4 protein was purified from *E. coli*. The PF4 or δsp-PF4 protein concentration was measured with an ELISA kit (human PF4/CXCL4 ELISA kit; Frankel, Shanghai, China).

Binding assay. RD cells were seeded in a 6-well plate for 16 h, the cell culture medium was removed, the cells were washed twice with cold PBS, and then 2 mL binding buffer (PBS containing 1% bovine serum albumin [BSA] and 0.1% sodium azide) was added to the cells (38). The cells were put on ice and incubated for 10 min and then removed from the binding buffer. Next, the RD cells were pretreated with IgG (500 ng/mL), anti-SCARB2 antibody (300 ng/mL), PF4 (10 ng/mL), or PF4 (10 ng/mL), and anti-PF4 antibody (220 ng/mL) for 2 h and then washed with PBS, and EV71 or CA16 were diluted in 2 mL DMEM and added to the cells at the indicated MOI. The cells were put on ice for 1 h before removing the virus and washed with PBS three times, and then the cells were lysed in TRIzol for RNA analysis.

Western blotting and antibodies. Virus-infected HEK293T or RD cells were lysed in 1× loading buffer (0.08 M Tris, pH 6.8, with 2.0% SDS, 10% glycerol, 0.1 M dithiothreitol, and 0.2% bromophenol blue) and boiled at 100°C for 30 min. After that, these samples were centrifuged at 12,000 × g for 10 min. The proteins were resolved by SDS-PAGE and transferred to polyvinylidene difluoride (PVDF) membranes for Western blotting. After blocking with 5% nonfat dry milk for 1 h at room temperature (RT), the membranes were incubated with primary antibodies at 4°C overnight, followed by corresponding horseradish peroxidase (HRP)-conjugated secondary antibody (Jackson Immunoresearch, West Grove, PA, USA) for 1 h at RT. Proteins were developed using an ultrasensitive ECL chemiluminescence detection kit (Proteintech, Rosemont, IL, USA; catalog number B500024).

The following antibodies were used in this study: polyclonal antibodies (pAbs) against EV71 (rabbit) and CA16 (mice) that have been described in previous articles (32, 33, 37), anti-SCARB2 antibody (Proteintech; catalog number 27102-1-AP, diluted 1:2,000), anti-PF4 antibody (Proteintech; catalog number 21157-1-AP, diluted 1:2,000), anti-hemagglutinin (anti-HA) pAb (Invitrogen; catalog number 71-5500, diluted 1:2,000), anti-Flag MAb (Sigma, St. Louis, MO, USA; catalog number F1804, diluted 1:2,500), anti-myc monoclonal antibody (MAb) (Millipore, Billerica, MA, USA; catalog number 05-724, diluted 1:1,000), and anti-tubulin MAb (Abcam, Cambridge, Cambridgeshire, UK; catalog number ab11323, diluted 1:2,000).

Coimmunoprecipitation assay. For VP3-HA IP, HEK293T cells were transfected with PF4-Flag and VP3-HA or VR1012 for 48 h. The cells were then harvested and washed twice with cold PBS followed by disruption with lysis buffer (50 mM Tris-HCl, pH 7.5, 150 mM NaCl, 0.5% NP40, and complete protease inhibitor cocktail [Roche]) at 4°C for 2 h. Cell lysates were clarified by centrifugation at 10,000 × *g* for 10 min at 4°C. Anti-HA agarose beads (Roche) were mixed with the precleared cell lysates and incubated at 4°C for 4 h on an end-over-end rocker. The reaction mixtures were then washed six times with cold wash buffer (20 mM Tris-HCl, pH 7.5, 100 mM NaCl, 0.1 mM EDTA, 0.05% Tween 20) and subsequently analyzed by IB. For PF4-Flag or δsp-PF4-Myc IP, Flag Ab or Myc Ab and protein G agarose beads (Roche) were incubated and used.

Neonatal mouse infection model. One-day-old specific pathogen-free (SPF) ICR neonatal mice were used to establish the animal model of viral infection. The neonatal mice were randomly divided into nine

groups, and each group contained three litters (n = 10 to 15 per litter). Four groups were inoculated intracerebrally with DMEM (10 μL/mouse), PF4 only (2 ng/mL, 10 μL/mouse), PF4 (2 ng/mL, 10 μL/mouse) and EV71 CC063 ($10^{5.5}$ $CCID_{50}$ mL^{-1}, 10 μL/mouse), or EV71 only ($10^{5.5}$ $CCID_{50}$ mL^{-1}, 10 μL/mouse), respectively. The other five groups were intracranially inoculated with premixed PF4 (2 ng/mL, 1 ng/mL, or 0.7 ng/mL; 9 μL/mouse) and the EV71 CC063 ($10^{6.5}$ $CCID_{50}$ mL^{-1}, 1 μL/mouse) for 1 h, EV71 only or DMEM as negative control. The survival rates and mean clinical symptoms were monitored daily for 15 days postinfection. The mean clinical symptoms were scored as follows: 0, healthy; 1, lethargy or weakness; 2, wasting; 3, limb tremors; 4, paralysis in hind limb; and 5, moribund or dead. The control mice were healthy throughout the experiment.

Viral loads in neonatal mouse tissues postchallenge. After intracerebral inoculation with EV71 CC063 viruses or negative control DMEM, three experimental neonatal mice and three neonatal control mice were subjected to viral load detection. The EV71 infection and control groups were collected on day 6 postinfection. All tissues, including brain, lung, spine skeletal muscle, and hind-limb muscle, were weighed individually, homogenized in sterile PBS, disrupted by freeze-thawing, and centrifuged. The samples were treated with TRIzol (Invitrogen) for RNA extraction and viral load determination by RT-qPCR as described previously (1, 37). Viral loads were expressed as $\log_{10}$ copies per milligram tissue.

Histopathological analysis. A total of 18 mice were sampled as follows: three normal mice from the negative control group (the clinical score of grade 0), three normal mice from the PF4-treated group (grade 0), three mice from the EV71-infected (grade 5), three mice from the EV71-infected and PF4 (2 ng/mL)-treated group (grade 2), three mice from the EV71-infected and PF4 (1 ng/mL)-treated group (grade 3), and three mice from the EV71-infected and PF4 (0.7 ng/mL)-treated group (grade 3). After the mice were anesthetized, lung, brain, spine skeletal muscle, and hind-limb muscle tissues were harvested and immersion fixed with 10% formaldehyde solution for 2 days. Then, all samples were dehydrated via an ethanol gradient, clarified through dimethyl benzene, embedded in paraffin, and 4-m sections were obtained for hematoxylin and eosin (H&E) staining. Histopathological analysis of the tissues was performed under a light microscope.

Washed platelet preparation. Platelet-rich plasma (PRP) obtained from the healthy individuals was centrifuged, and the platelets were resuspended in calcium-free Tyrode buffer (Sigma-Aldrich, St. Louis, MO, USA).

Statistical analysis. The data were analyzed using Microsoft Excel with the Student's t test (two-tailed). Differences were considered statistically significant at the following P values: **, $P < 0.01$; ***, $P < 0.001$; ****, $P < 0.0001$. Kaplan-Meier survival curves were analyzed using a log-rank test.

Ethics statement. All animal experiments were performed following the Animal Experiment Center of Basic Medicine School of Jilin University. All efforts were made to minimize suffering. The protocol was approved by the Animal Experiment Center of Basic Medicine School of Jilin University (license number 2021-152). The plasma samples from healthy volunteers were approved by the ethics committee at the First Hospital of Jilin University (license number 19K029-001).

ACKNOWLEDGMENTS

We thank C. Y. Dai for the critical reagents.

This work was supported in part by funding from the National Key R&D Program of China (2021YFC2301900 and 2301904), the National Natural Science Foundation of China (numbers 81930062, and 81672004), the Department of Science and Technology of Jilin Province (20190201272JC), and Key Laboratory of Molecular Virology, Jilin Province (20102209).

We declare no conflicts of interest.

REFERENCES

1. Handin RI, Cohen HJ. 1976. Purification and binding properties of human platelet factor four. J Biol Chem 251:4273–4282. https://doi.org/10.1016/S0021-9258(17)33292-1.
2. Levine SP, Wohl H. 1976. Human platelet factor 4: purification and characterization by affinity chromatography. Purification of human platelet factor 4. J Biol Chem 251:324–328. https://doi.org/10.1016/S0021-9258(17)33882-6.
3. Broos K, Feys HB, De Meyer SF, Vanhoorelbeke K, Deckmyn H. 2011. Platelets at work in primary hemostasis. Blood Rev 25:155–167. https://doi.org/10.1016/j.blre.2011.03.002.
4. Clemetson KJ. 2012. Platelets and primary haemostasis. Thromb Res 129:220–224. https://doi.org/10.1016/j.thromres.2011.11.036.
5. Gawaz M, Vogel S. 2013. Platelets in tissue repair: control of apoptosis and interactions with regenerative cells. Blood 122:2550–2554. https://doi.org/10.1182/blood-2013-05-468694.
6. Golebiewska EM, Poole AW. 2015. Platelet secretion: from haemostasis to wound healing and beyond. Blood Rev 29:153–162. https://doi.org/10.1016/j.blre.2014.10.003.
7. Jennings LK. 2009. Role of platelets in atherothrombosis. Am J Cardiol 103:4A–10A. https://doi.org/10.1016/j.amjcard.2008.11.017.
8. Kaplan ZS, Jackson SP. 2011. The role of platelets in atherothrombosis. Hematology Am Soc Hematol Educ Program 2011:51–61. https://doi.org/10.1182/asheducation-2011.1.51.
9. Sabrkhany S, Griffioen AW, Oude Egbrink MG. 2011. The role of blood platelets in tumor angiogenesis. Biochim Biophys Acta 1815:189–196. https://doi.org/10.1016/j.bbcan.2010.12.001.
10. Semple JW, Italiano JE, Jr, Freedman J. 2011. Platelets and the immune continuum. Nat Rev Immunol 11:264–274. https://doi.org/10.1038/nri2956.
11. Thomas MR, Storey RF. 2015. The role of platelets in inflammation. Thromb Haemost 114:449–458. https://doi.org/10.1160/TH14-12-1067.
12. Walsh TG, Metharom P, Berndt MC. 2015. The functional role of platelets in the regulation of angiogenesis. Platelets 26:199–211. https://doi.org/10.3109/09537104.2014.909022.
13. Singh A, Bisht P, Bhattacharya S, Guchhait P. 2020. Role of platelet cytokines in dengue virus infection. Front Cell Infect Microbiol 10:561366. https://doi.org/10.3389/fcimb.2020.561366.
14. Auerbach DJ, Lin Y, Miao H, Cimbro R, Difiore MJ, Gianolini ME, Furci L, Biswas P, Fauci AS, Lusso P. 2012. Identification of the platelet-derived chemokine CXCL4/PF-4 as a broad-spectrum HIV-1 inhibitor. Proc Natl Acad Sci U S A 109:9569–9574. https://doi.org/10.1073/pnas.1207314109.
15. Guo L, Feng K, Wang YC, Mei JJ, Ning RT, Zheng HW, Wang JJ, Worthen GS, Wang X, Song J, Li QH, Liu LD. 2017. Critical role of CXCL4 in the lung pathogenesis of influenza (H1N1) respiratory infection. Mucosal Immunol 10:1529–1541. https://doi.org/10.1038/mi.2017.1.
16. Han Z, Rao J, Xie Z, Wang C, Xu B, Qian S, Wang Y, Zhu J, Yang B, Xu F, Lei X, Guo F, Zhao Z, Ren L, Wang J. 2020. Chemokine (C-X-C Motif) ligand 4

is a restrictor of respiratory syncytial virus infection and an indicator of clinical severity. Am J Respir Crit Care Med 202:717–729. https://doi.org/10.1164/rccm.201908-1567OC.
17. Ojha A, Bhasym A, Mukherjee S, Annarapu GK, Bhakuni T, Akbar I, Seth T, Vikram NK, Vrati S, Basu A, Bhattacharyya S, Guchhait P. 2019. Platelet factor 4 promotes rapid replication and propagation of dengue and Japanese encephalitis viruses. EBioMedicine 39:332–347. https://doi.org/10.1016/j.ebiom.2018.11.049.
18. Ojha A, Nandi D, Batra H, Singhal R, Annarapu GK, Bhattacharyya S, Seth T, Dar L, Medigeshi GR, Vrati S, Vikram NK, Guchhait P. 2017. Platelet activation determines the severity of thrombocytopenia in dengue infection. Sci Rep 7:41697. https://doi.org/10.1038/srep41697.
19. Parker ZF, Rux AH, Riblett AM, Lee FH, Rauova L, Cines DB, Poncz M, Sachais BS, Doms RW. 2016. Platelet factor 4 inhibits and enhances HIV-1 infection in a concentration-dependent manner by modulating viral attachment. AIDS Res Hum Retroviruses 32:705–717. https://doi.org/10.1089/AID.2015.0344.
20. Schwartzkopff F, Grimm TA, Lankford CS, Fields K, Wang J, Brandt E, Clouse KA. 2009. Platelet factor 4 (CXCL4) facilitates human macrophage infection with HIV-1 and potentiates virus replication. Innate Immun 15:368–379. https://doi.org/10.1177/1753425909106171.
21. Shukla D, Liu J, Blaiklock P, Shworak NW, Bai X, Esko JD, Cohen GH, Eisenberg RJ, Rosenberg RD, Spear PG. 1999. A novel role for 3-O-sulfated heparan sulfate in herpes simplex virus 1 entry. Cell 99:13–22. https://doi.org/10.1016/s0092-8674(00)80058-6.
22. Tan CW, Poh CL, Sam IC, Chan YF. 2013. Enterovirus 71 uses cell surface heparan sulfate glycosaminoglycan as an attachment receptor. J Virol 87:611–620. https://doi.org/10.1128/JVI.02226-12.
23. Baggen J, Thibaut HJ, Strating J, van Kuppeveld FJM. 2018. The life cycle of non-polio enteroviruses and how to target it. Nat Rev Microbiol 16:368–381. https://doi.org/10.1038/s41579-018-0005-4.
24. Brown DM, Zhang Y, Scheuermann RH. 2020. Epidemiology and sequence-based evolutionary analysis of circulating non-polio enteroviruses. Microorganisms 8:1856. https://doi.org/10.3390/microorganisms8121856.
25. Zhou D, Zhao Y, Kotecha A, Fry EE, Kelly JT, Wang X, Rao Z, Rowlands DJ, Ren J, Stuart DI. 2019. Unexpected mode of engagement between enterovirus 71 and its receptor SCARB2. Nat Microbiol 4:414–419. https://doi.org/10.1038/s41564-018-0319-z.
26. Dang M, Wang X, Wang Q, Wang Y, Lin J, Sun Y, Li X, Zhang L, Lou Z, Wang J, Rao Z. 2014. Molecular mechanism of SCARB2-mediated attachment and uncoating of EV71. Protein Cell 5:692–703. https://doi.org/10.1007/s13238-014-0087-3.
27. Yamayoshi S, Iizuka S, Yamashita T, Minagawa H, Mizuta K, Okamoto M, Nishimura H, Sanjoh K, Katsushima N, Itagaki T, Nagai Y, Fujii K, Koike S. 2012. Human SCARB2-dependent infection by coxsackievirus A7, A14, and A16 and enterovirus 71. J Virol 86:5686–5696. https://doi.org/10.1128/JVI.00020-12.
28. Kobayashi K, Koike S. 2020. Cellular receptors for enterovirus A71. J Biomed Sci 27:23. https://doi.org/10.1186/s12929-020-0615-9.
29. Nishimura Y, Shimojima M, Tano Y, Miyamura T, Wakita T, Shimizu H. 2009. Human P-selectin glycoprotein ligand-1 is a functional receptor for enterovirus 71. Nat Med 15:794–797. https://doi.org/10.1038/nm.1961.
30. Yang SL, Chou YT, Wu CN, Ho MS. 2011. Annexin II binds to capsid protein VP1 of enterovirus 71 and enhances viral infectivity. J Virol 85:11809–11820. https://doi.org/10.1128/JVI.00297-11.
31. Wei W, Guo H, Chang J, Yu Y, Liu G, Zhang N, Willard SH, Zheng S, Yu XF. 2016. ICAM-5/telencephalin is a functional entry receptor for enterovirus D68. Cell Host Microbe 20:631–641. https://doi.org/10.1016/j.chom.2016.09.013.
32. Chang J, Li J, Wei W, Liu X, Liu G, Yang J, Zhang W, Yu XF. 2015. Determinants of EV71 immunogenicity and protection against lethal challenge in a mouse model. Immunol Res 62:306–315. https://doi.org/10.1007/s12026-015-8661-1.
33. Li J, Chang J, Liu X, Yang J, Guo H, Wei W, Zhang W, Yu XF. 2014. Protection from lethal challenge in a neonatal mouse model by circulating recombinant form coxsackievirus A16 vaccine candidates. J Gen Virol 95:1083–1093. https://doi.org/10.1099/vir.0.063560-0.
34. Fu X, Wan Z, Li Y, Hu Y, Jin X, Zhang C. 2020. National epidemiology and evolutionary history of four hand, foot and mouth disease-related enteroviruses in China from 2008 to 2016. Virol Sin 35:21–33. https://doi.org/10.1007/s12250-019-00169-2.
35. Xiang Z, Li L, Ren L, Guo L, Xie Z, Liu C, Li T, Luo M, Paranhos-Baccala G, Xu W, Wang J. 2017. Seroepidemiology of enterovirus D68 infection in China. Emerg Microbes Infect 6:e32. https://doi.org/10.1038/emi.2017.14.
36. Anasir MI, Zarif F, Poh CL. 2021. Antivirals blocking entry of enteroviruses and therapeutic potential. J Biomed Sci 28:10. https://doi.org/10.1186/s12929-021-00708-8.
37. Xu N, Yang J, Zheng B, Zhang Y, Cao Y, Huan C, Wang S, Chang J, Zhang W. 2020. The Pyrimidine analog FNC potently inhibits the replication of multiple enteroviruses. J Virol 94:e00204-20. https://doi.org/10.1128/JVI.00204-20.
38. He QQ, Ren S, Xia ZC, Cheng ZK, Peng NF, Zhu Y. 2018. Fibronectin facilitates enterovirus 71 infection by mediating viral entry. J Virol 92:e02251-17. https://doi.org/10.1128/JVI.02251-17.